SAND2021-15092C

Validation Study of the Multi-Fidelity Toolkit

Blake W. Lance*, Aaron M. Krueger†, Brian A. Freno‡, and Ross M. Wagnild§
Sandia National Laboratories, Albuquerque, NM, 87123

The Multi-Fidelity Toolkit (MFTK) is a simulation tool being developed at Sandia National Laboratories for aerodynamic predictions of compressible flows over a range of physics fidelities and computational speeds. These models include the Reynolds-Averaged Navier–Stokes (RANS) equations, the Euler equations, and modified Newtonian aerodynamics (MNA) equations, and they can be invoked independently or coupled with hierarchical Kriging to interpolate between high-fidelity simulations using lower-fidelity data. However, as with any new simulation capability, verification and validation are necessary to gather credibility evidence. This work describes formal model validation with uncertainty considerations that leverages experimental data from the HIFiRE-1 wind tunnel tests. The geometry is a multi-conic shape that produces complex flow phenomena under hypersonic conditions. A thorough treatment of the validation comparison with prediction error and validation uncertainty is also presented.

I. Introduction

The Multi-Fidelity Toolkit (MFTK) is a suite of tools being developed at Sandia National Laboratories to improve the response time for aerothermodynamic queries for hypersonic flight vehicles. The toolkit comprises three levels of aerothermodynamic physics fidelity and a series of file- and data-handling scripts: an input-file generator, a sample-point dispatcher, a data-gathering code, and a multi-fidelity interpolation code. The aerothermodynamic evaluation fidelity levels are being developed in the Sandia Parallel Aerodynamics and Reentry Code (SPARC) and consist of a modified Newtonian aerodynamics (MNA) solver, an Euler solver, and a Reynolds-Averaged Navier–Stokes (RANS) solver. The low- and medium-fidelity models do not have the ability to compute viscous effects such as heat flux; therefore, both transfer data to different correlation-based models. The multi-fidelity interpolation code uses a hierarchical Kriging method [1] to perform sample evaluations over a parameter space by using trends from lower-fidelity predictions and anchoring to high-fidelity predictions, such as those from a RANS solver. This allows for more accurate predictions to be computed over a large parameter space at a reduced cost, compared to running a RANS solver only. With the multi-fidelity interpolation method, the focus of the lower-fidelity methods is on minimizing the error in the trend of aerothermodynamic data rather than the absolute error of each model. However, achieving the expected order of accuracy is necessary to ensure the lower-fidelity models have been correctly implemented.

To assess the credibility of predictions using MFTK, verification and validation activities are performed to ensure the correct implementation and appropriate use of the models. Verification activities are not documented herein but in an accompanying paper [2]. Validation assesses how well the implemented models represent the relevant physical phenomena. This is typically done by comparing simulation predictions with experimental data to assess the modeling error and ultimately the bounds of validity for a defined application space. By contrast, verification is, according to the American Society of Mechanical Engineers (ASME) Standard for Verification and Validation in Computational Solid Mechanics [3], "the process of determining that a computational model accurately represents the underlying model and its solution." Verification is further broken up into code verification and solution verification [4–6]. Code verification focuses on the correct implementation of the mathematical model, whereas solution verification focuses on estimating the numerical error for a particular solution.

Model validation is defined by both the American Institute of Aeronautics and Astronautics (AIAA) "Guide for Verification and Validation of Computational Fluid Dynamics Simulations" and the ASME "Standard for Verification and Validation in Computational Fluid Dynamics and Heat Transfer" as, "the process of determining the degree to which a model is an accurate representation of the real world from the perspective of the intended uses of the model." [7, 8].

*Senior Member of the Technical Staff; V&V, UQ, and Credibility Processes Department; AIAA Member; Corresponding Author: blance@sandia.gov
†Senior Member of the Technical Staff; V&V, UQ, and Credibility Processes Department
‡Senior Member of the Technical Staff; V&V, UQ, and Credibility Processes Department; AIAA Senior Member
§Principal Member of the Technical Staff, Aerosciences Department, AIAA Senior Member

The scope of this work does not include the multi-fidelity interpolation aspect of MFTK because it is applied to a single parameter set for the validation case instead of a parameter exploration. Instead, predictions are made at each fidelity level independently to assess predictive accuracy, with the understanding that lower-fidelity models are expected to have lower accuracy. The low-fidelity MNA model may occasionally be executed independently, but its main purpose is to predict trend information with many runs across a parameter sweep. The mid-fidelity Euler solver may be run independently for quick-turnaround simulations or potentially in a Monte Carlo-style uncertainty quantification (UQ) analysis, so predictive accuracy is more desirable and expected here.

II. Model Validation Theory

Though formally defined in the introduction, informally, model validation seeks to determine the degree to which the model is solving the physically appropriate equations. For high-speed aerodynamics, these would include compressible forms of the continuity, momentum, and energy equations. For the turbulent flows, including the full forms of the governing equations (as in Direct Numerical Simulation) is often not tractable; therefore, closure models are frequently used (as in RANS). The inviscid treatment of certain flows is another example of a modeling assumption. Model validation processes can be used to determine the suitability of such modeling assumptions.

Comparing simulation predictions to experimental results is fundamental to model validation. There are several levels of scrutiny in comparisons that are seen in literature. A helpful comparison is found in Fig. 12 of [9] that presents six levels of validation comparisons. The first and least descriptive is the viewgraph norm where contours are placed next to each other, but differences in values are often obscured from the wealth of field information and colorful scales. The next plots show several levels of comparisons that switch to a common set of axes that are much better at revealing direct information. Increasing the levels of UQ on measurements and predictions increases the rigor.

The ASME V&V 20 standard goes beyond comparisons in plots to the calculation of validation comparison error and the validation uncertainty [8]. In this standard, the validation comparison error E is defined as

$$E = S - D, \tag{1}$$

where S represents the simulation solution and D represents the experimental data. Equation (1) provides the simplest validation metric, which nonetheless transitions from the qualitative comparisons in plots to a quantitative measure used to evaluate predictive accuracy. It can be used to reveal trends in model form error over space, time, or parameter sets.

The validation comparison error reveals differences, but how meaningful are those differences, and could experimental and/or modeling uncertainties explain them? To help answer these questions, ASME V&V 20 also includes the calculation of a validation uncertainty

$$u_{\text{val}} = \sqrt{u_{\text{num}}^2 + u_{\text{input}}^2 + u_D^2}, \tag{2}$$

where u_{num} is the numerical uncertainty commonly assessed by grid convergence studies, u_{input} is the input parameter uncertainty propagated through the model, and u_D is the experimental data uncertainty [8]. Equation (2) is in the form of a standard uncertainty at the 1σ or 68% confidence level. To calculate the expanded uncertainty at a more typical 2σ or 95% confidence level, the confidence coefficient $C = 2$ can be included as in $U = Cu$ on the uncertainty components or on u_{val}. Throughout this work, uncertainties are presented at the 95% confidence level.

The validation uncertainty provides perspective on the validation error. For example, if $|E| \gg u_{\text{val}}$, then model form error is discernible from the relatively small validation uncertainty and model improvements may be prudent if the errors are larger than desired. On the other hand, if $|E| \leq u_{\text{val}}$, model form error is not distinguishable among the validation uncertainty and efforts to reduce uncertainty may be pertinent.

Note that E is the validation comparison error and includes possible errors in measured data and simulation predictions. It is, therefore, not the model form error. The exact model form error is challenging to isolate but can be bounded. In ASME V&V 20 [8], the model form error is bounded by

$$\delta_{\text{model}} \in [E - u_{\text{val}}, E + u_{\text{val}}]. \tag{3}$$

This bounding motivates efforts to minimize uncertainty in both experiments and simulations so that the model form error can be known with greater accuracy.

III. HIFiRE-1 Wind Tunnel Tests

Experimental data are critical to validation studies, but there are few presented in the public literature for hypersonic aerodynamic vehicles, possibly due to the challenges of measurements under these extreme conditions or the sensitivities of the applications. There are a handful of tests that include a mix of flight and ground tests. These two types have benefits and drawbacks. Flights tests are closer to the intended uses of MFTK, but measurement quantity and quality for aero-only quantities are challenging. Most flight tests of hypersonic vehicles require a thermal protection system that complicates the direct measurement of aerodynamic quantities such as surface pressure, temperature, and heat flux. Also, flight test conditions are only loosely controlled and measured. Conversely, ground tests are farther from the intended uses of MFTK but enable greater instrumentation and control of conditions. Many ground test facilities are shock tunnels that induce hypersonic conditions for a fraction of a second, eliminating the need for thermal protection systems.

Many potential validation data sources were surveyed for this work. One source of hypersonic aerodynamic validation data is the Hypersonic International Flight Research and Experimentation (HIFiRE) program that sought to develop hypersonic technologies. The program included atmospheric flight tests and ground tests in the shock tunnel facilities at the Calspan–University at Buffalo Research Center (CUBRC). Their Large Energy National Shock (LENS) facilities include LENS I, LENS II, and LENS XX [10]. Of particular interest are the HIFiRE-1 wind tunnel tests that have been used for validation data in a number of subsequent publications that were conducted in the LENS I shock tunnel [11].

The HIFiRE-1 wind tunnel tests were selected for a validation application due to hypersonic flow conditions, challenging flow characteristics, turbulence, testing with air, and a wealth of high-quality data that spans a range of angles of attack and Reynolds numbers [11]. One down-side is the low enthalpy conditions in the flow that will not exercise the reacting gas models in the MFTK RANS implementation. The HIFiRE-1 flight test was not selected due to the coning motion during reentry that makes it less ideal for validation [12].

The HIFiRE-1 wind tunnel geometry is shown in Fig. 1. It has a complex shape with a slender 7° half-angle fore-cone, a cylindrical section in the center, then a blunt flare at the rear. Depending on the run configuration, turbulent transition occurs naturally or is tripped on the fore-cone. The flare causes a separation bubble in the cylindrical section that is a challenge for many RANS models [10]. The test series had a total of over 50 runs in two phases and the model contains a total of almost 100 heat flux sensors and 56 pressure sensors that are located at four different meridional angles.

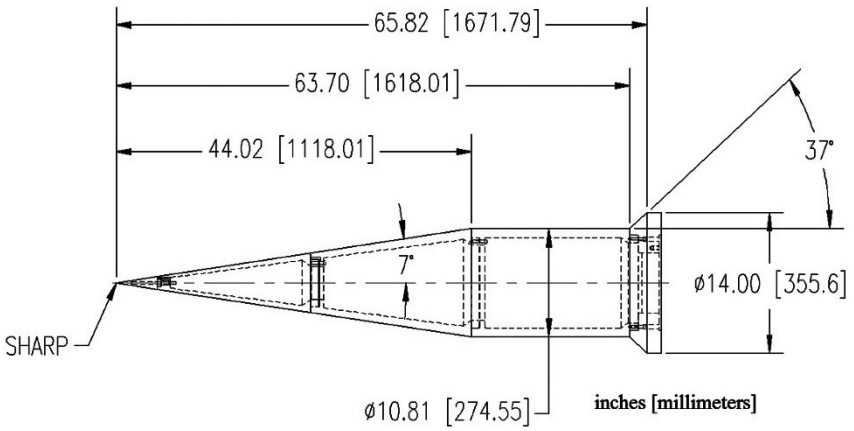

Fig. 1 The HIFiRE-1 wind tunnel test geometry that shows the fore-cone on the left, the cylindrical section in the center, and the flare on the right, from [11]. The text states that the final nosetip was changed from sharp to a radius of 2.5 mm and the flare angle was changed from 37° to 33°.

To provide a sense of the flow field, the Mach number predictions in a two-dimensional, axisymmetric, wall-normal plane for two RANS models are shown in Fig. 2. The flow is left to right. The solid wind tunnel model is the white region in the lower right and includes the cone, the cylinder, and the flare. The white region in the upper left is not simulated. The RANS Spalart–Allmaras (SA) and RANS Shear Stress Transport (SST) models predict similar flow fields with the exception of the separated region near the cylinder-flare intersection that is more pronounced for RANS-SST.

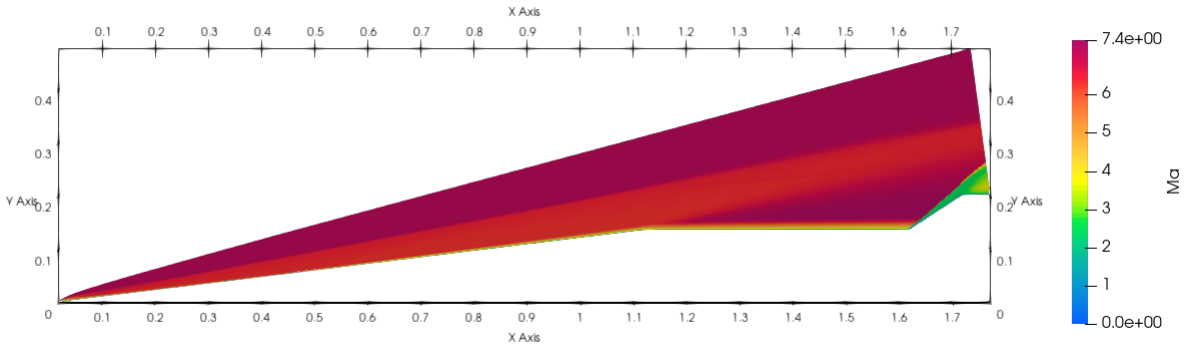

(a) RANS-SA

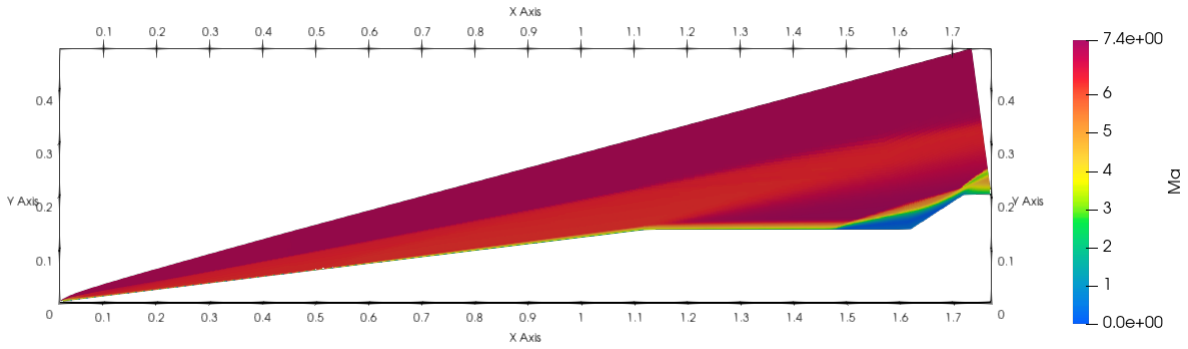

(b) RANS-SST

Fig. 2 HIFiRE-1 wind tunnel simulation Mach number predictions for RANS-SA and RANS-SST models.

IV. Validation Results

The validation studies herein include surface pressure and heat flux comparisons for Run 30, a 0° angle-of-attack case at a relatively high Reynolds number. In addition to traditional comparison plots, the validation comparison error E from (1) and validation uncertainty u_{val} from (2) are calculated and plotted to enable quantitative comparisons of predictive accuracy at all three fidelity levels of MFTK. The experimental data have known uncertainties [11]. Similarly, the solution-verification studies in the companion paper [2] provide numerical uncertainty values u_{num}. Note that for all of the simulation results herein, the medium mesh was used and iterative convergence was achieved by driving normalized residuals below 10^{-12}. The parameter uncertainty u_{input} is not calculated in this work but recommended for future work.

A. Surface Pressure Comparisons

The first validation comparison is the surface pressure along the axial length of the vehicle as shown in Fig. 3. The test vehicle geometry is shown with the second y axis as a gray region to provide background to the drastically different behavior along the length. The results include measured data and predictions from the RANS-SA model, the RANS-SST model, the Euler model combined with the Momentum/Energy Integral Technique (MEIT), and the modified Newtonian aerodynamics (MNA) model combined with flat-plate boundary layer (FPBL) correlations. The experimental pressure uncertainty is 3% [11], interpreted as 3% of reading in the associated error bars/uncertainty bands. The simulations have numerical uncertainty from the GCI results from solution verification shown as shaded regions that are colored according to their respective model color. The data are taken from the 0° meridian that has the most sensors. The fore-cone has very few pressure sensors, but the pressure is nearly constant in this region. The instrumentation density increases towards the rear of the vehicle where the flow is more complex. The pressures increase drastically on the 33° flare region. The predictions used meshes that were derived from the same source. From a 3D source mesh, a 2D axisymmetric mesh with 131,072 cells was derived for the RANS and Euler+MEIT simulations. For the MNA model, which only requires a surface mesh, the 3D surface was extracted from the source mesh.

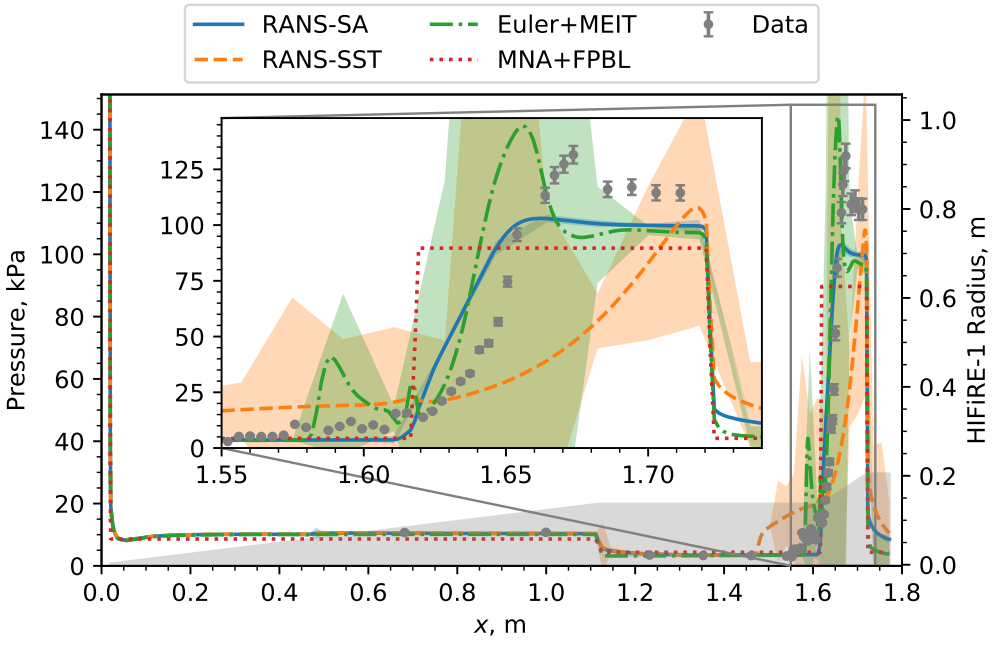

Fig. 3 HIFiRE-1 wind tunnel test pressure data and predictions.

This figure features an inset plot that highlights the aft end of the cylindrical and the flare regions where the pressure measurements and predictions are quite complex. The RANS predictions compare very well on the fore-cone and cylinder sections, as expected due to the inviscid nature of the surface pressure. However, the agreement breaks down at the separation point leading to the flare, which highlights the known inability of RANS models to capture the complex

physics of turbulent flow through a shock/boundary layer interaction [13]. The SA model generally predicts pressure more accurately in this region, though it appears to miss the physics of separation. The SST model over-predicts the separation region, consistent with the findings of modelers associated with the HIFiRE study [10]. The RANS-SA model has low numerical uncertainty while the RANS-SST model has a very large uncertainty as the pressure predictions change drastically in the separation and flare regions.

While others at Sandia National Laboratories have recently completed validation studies with RANS in a similar manner [13], the mid-fidelity Euler+MEIT and low-fidelity MNA+FPBL models have undergone no known validation work. Similar to the two RANS models, the Euler+MEIT predictions are also qualitatively very good in the fore-cone and cylinder sections. The pressure predictions more closely align with those from the SA model in the separation region, though with some noise along the axis. Interestingly, it appears that this mid-fidelity model combination is more accurate than the SST model near this separation. However, the mid-fidelity model is not mesh-converged as evidenced by the large numerical uncertainty. Quantitative comparisons follow herein that present greater detail.

The surface pressure predictions of the MNA+FPBL are also of high interest. Because MNA is one of the class of so-called 'panel' methods, the only means by which it computes the surface pressure is by using analytic formulas to process the flow through a shock wave and then deflect the flow at the angle of the panel on the surface. These two steps dictate the surface pressure on any forward-facing panel in the solver. The theoretical concept of panel methods, flow deflection without losses or viscous modification, is reasonably true in the limit of infinite Mach and Reynolds numbers and thus is only an approximation at finite values. With this in mind, the MNA solver does a reasonable job predicting the surface pressure on the fore-cone and cylindrical portions of the vehicle. The MNA solver does not model any shock waves or boundary layers and is incapable of predicting the separation point observed in the experiments. The flare portion of the vehicle presents a higher degree of deflection compared to the rest of the vehicle and therefore shows the highest surface pressure, aside from the stagnation point on the nose. The MNA+FPBL models predict the increase in surface pressure at the flare with reasonable accuracy, but do not capture the non-uniform behavior observed in the experiment. The numerical uncertainty is negligible because this model is a panel method for which the pressure predictions are only a function of inflow and the angle between the panel and the flow.

To determine quantitative accuracy, the errors in surface pressure predictions were calculated using (1) and normalized by the experimental data for the four models along the vehicle axis and shown in Fig. 4. The error is very low in the fore-cone and cylindrical sections as expected with the MNA+FPBL models showing the largest error. The error increases greatly in the separation and flare region with strong positive and negative errors. The validation uncertainty calculated from (2), with $u_{\text{input}} = 0$, is also shown as a shaded band to help determine if the validation error is discernible among the uncertainty, which it clearly is for the RANS-SA and MNA+FPBL models but not consistently for others.

Because the validation error along the axis is very noisy with large differences in magnitude in different sections, overall conclusions may be challenging to formulate. To compensate for this, the validation error relative to the experimental data was averaged across all experimental data points for each model independently and plotted in a bar plot in Fig. 5. Figure 5a only includes the experimental uncertainty of 3%, whereas Fig. 5b includes both experimental and numerical uncertainty sources. The accuracy is better shown in Fig. 5a. Here, the improved accuracy of the SA model is shown with the subsequent models being Euler+MEIT, MNA+FPBL, and finally SST. The surprisingly high error of SST is due to the over-prediction of the separation region size where the data are relatively low. Again, the validation uncertainty is shown but in the form of uncertainty bands/error bars. If the experimental uncertainty were the only source, the errors would be distinguishable among the uncertainty calculated. However, as Fig. 5b shows, the validation uncertainty dominates for the RANS-SST and Euler+MEIT models, such that the error is not discernible. However, it is still distinguishable for the other two models.

The HIFiRE-1 geometry has several different sections that cause the flow to have different behavior, allowing us to evaluate the prediction error in multiple scenarios from the same data set. The pressure error is therefore averaged over sections of a cone with laminar and turbulent portions, a turbulent cylinder, and a turbulent flare with flow separation. The prediction error relative to experimental data is shown for these sections for all four model combinations in Fig. 6, except that there are no pressure measurements in the laminar section. Figure 6a provides a better look at prediction error by only considering the experimental uncertainty in the validation uncertainty. A more complete understanding is obtained from Fig. 6b where the validation uncertainty includes both experimental and numerical sources.

The pressure predictions are much more accurate in the turbulent cone section than the cylindrical or flare sections, suggesting that the flow separation is, in general, more challenging to model. In the turbulent cone section, the higher-fidelity models tend to provide the lowest errors. In the cylindrical section, interestingly, the RANS-SA and MNA+FPBL model combinations have the most accurate pressure predictions. Note here that the MNA+FPBL model

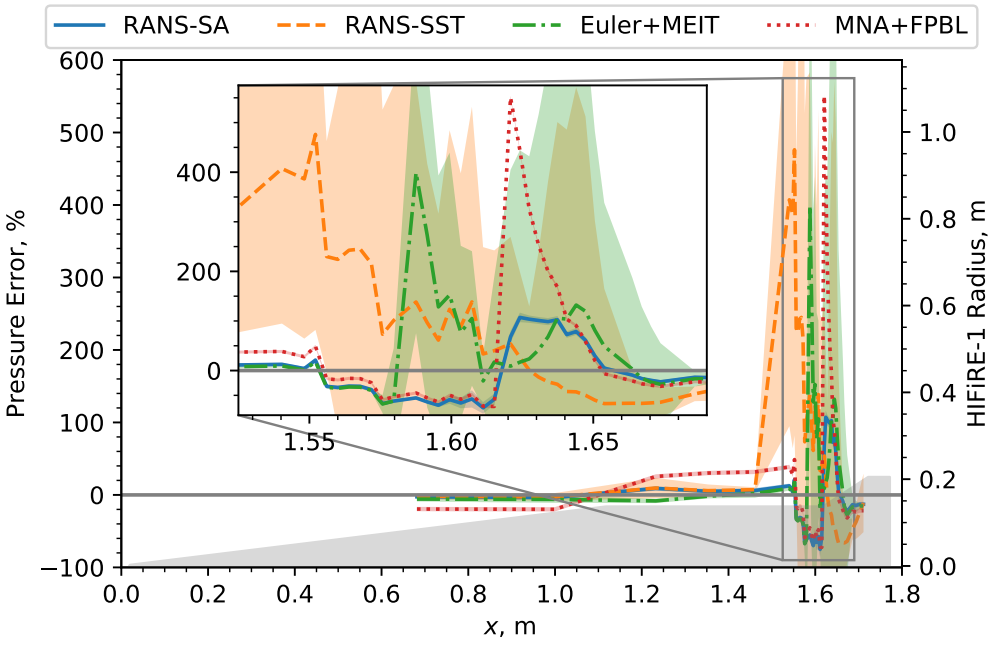

Fig. 4 HIFiRE-1 pressure prediction error with uncertainty.

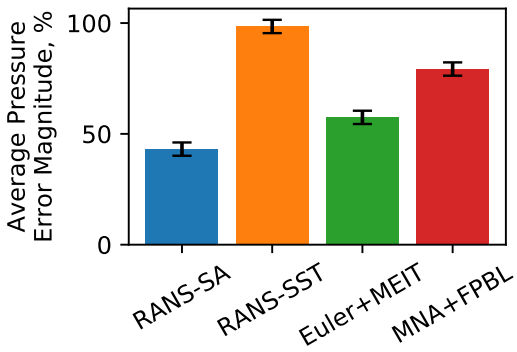

(a) Validation uncertainty only considering experimental source.

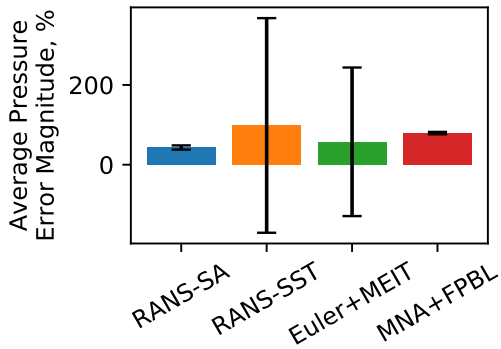

(b) Validation uncertainty considering experimental and numerical sources.

Fig. 5 HIFiRE-1 pressure prediction error magnitude averaged over data with uncertainty.

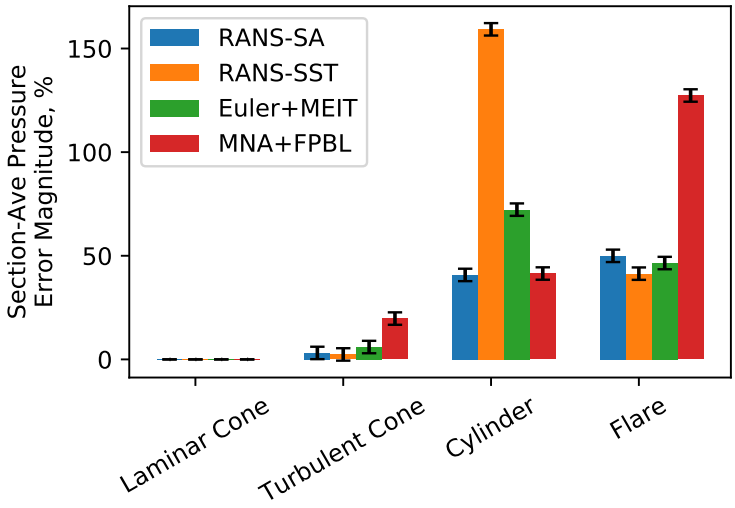

(a) Validation uncertainty only considering experimental source.

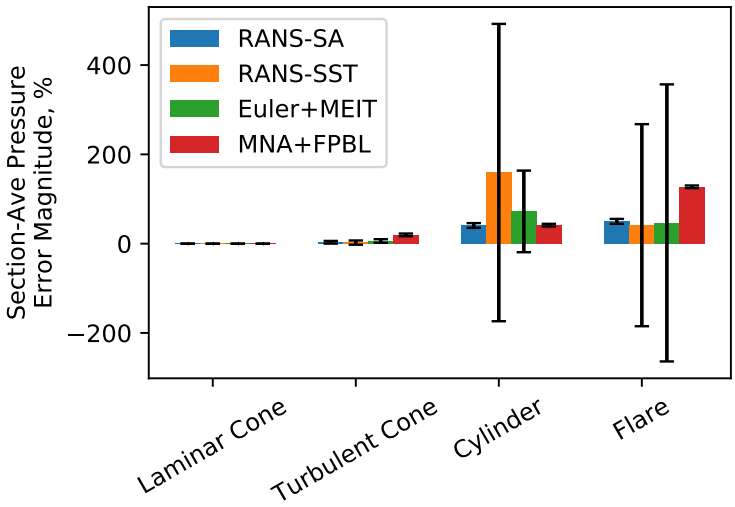

(b) Validation uncertainty considering experimental and numerical sources.

Fig. 6 HIFiRE-1 pressure prediction error magnitude separated by section with uncertainty.

combination does well here as the cylinder closely resembles a flat plate for which the viscous correlations were derived [14]. The RANS-SST model over-predicts the pressure in the separation region where the experimental data are relatively low. In the flare section, the three higher-fidelity models are the most accurate.

B. Surface Heat Flux Comparisons

The heat flux comparisons are shown in Fig. 7. Compared with pressure, there are many more sensors and there is an obvious transition from laminar to turbulent flow around $x = 0.45$ m. The experimental heat flux uncertainty is 5% [11]. The numerical uncertainty from solution verification is shown for each model as a shaded band. The RANS solutions do well in capturing both the laminar and turbulent heating on the fore-cone and cylinder. The transition between the boundary layer flow types is enacted by turning on the turbulence production terms at the approximate transition point on the fore-cone. The result of this method is to affect the change of laminar-to-turbulent transition heat flux over a much shorter duration than observed in the experiment. Additionally, the overshoot observed in the data is also missed by the simple transition method. As discussed previously, the separation point location is early in the RANS solution; however, the peak heat flux is consistent with the experimental data. The approach of manually setting the transition location was taken so that the focus is on the predictive accuracy of the physics models, not on the accuracy of a model to predict the transition location, an area that merits further research outside the scope of this work. The numerical uncertainty for the RANS-SA model is generally small throughout, except near the laminar-to-turbulent transition location. Conversely, this uncertainty for the RANS-SST model can be quite large, especially in the turbulent cone section, the aft end of the cylinder, and the flare (of which the latter two are in the predicted separation region).

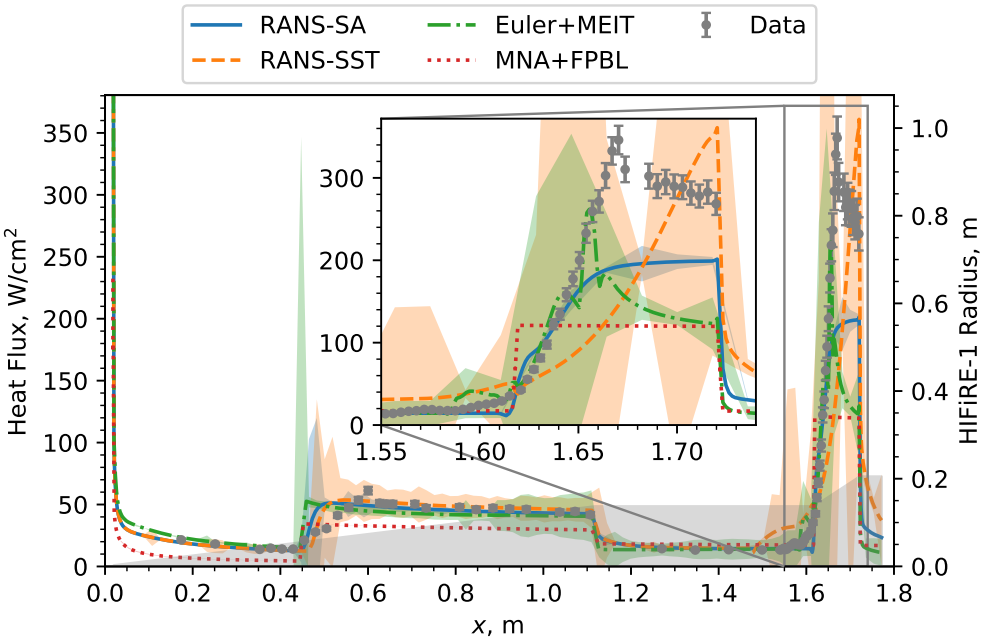

Fig. 7 HIFiRE-1 wind tunnel test heat flux data and predictions.

The Euler+MEIT model combination predictions are very reasonable considering their medium-physics fidelity. The predictive accuracy is nearly as good as the RANS models in the conical section and nearly identical in the cylinder section (except where the RANS-SST model predicts a larger separation bubble on the aft end). The predictions also match data very well on the fore end of the ramp but decrease too early with an error of about $2\times$. However, even with this premature decrease, the trend is correct and even better than either RANS model prediction. The numerical uncertainty can be moderately large, especially for $x > 0.9$ m. Note that, as with the RANS models, a laminar version of the model was used upstream of $x = 0.45$ m, and a turbulent version was used downstream.

The MNA+FPBL solver uses a flat-plate boundary layer correlation, a standard laminar correlation, and the Van Driest model for turbulent flow [15] to predict heat flux. As the conical geometry is somewhat removed from a flat plate,

it should be expected to have an error of at least $\sqrt{3}$ from the theoretical differences in heat flux. Future implementations of the boundary layer correlations may be targeted toward curvature-aware correlations to reduce this error. However, for the current implementation, the laminar heat flux has an error on the order of $2\times$ from the experiment over the laminar section of the fore-cone. As done with previous models, the laminar and turbulent models were applied fore and aft of $x = 0.45$ m, respectively. Interestingly, the heat flux nearly matches the experiment over the cylinder section of the vehicle, where the flat-plate correlation is very reasonable. On the flare, the error in heat flux is on the order of $3\times$, which is decent considering the complex fluid dynamics over the flare that are not modeled with the MNA model. Note the nearly flat shape of the heat flux prediction on the ramp where this model does not resolve the complex flow separation. As before, the MNA+FPBL numerical uncertainty is negligible.

As with surface pressure, the heat flux tends to have a lot of variation that can obscure quantitative accuracy conclusions. Therefore, the prediction error with validation uncertainty clouds for all four model combinations is shown in Fig. 8. Experimental data are available farther upstream than for pressure, into the laminar cone section of the domain. Accurate predictions in this laminar region are made by all but the MNA+FPBL model which under-predicts the heat flux. In the laminar-to-turbulent transition region, the prediction errors trend from positive to negative and tend to remain slightly negative in the turbulent cone section. In the cylinder section, all models show a high degree of accuracy. Similar to pressure, the errors tend to be largest in the flare region. The uncertainty cloud includes both the experimental and numerical uncertainty from (2), of which the latter dominates. Similar to pressure, the validation uncertainty is largest for the RANS-SST and Euler+MEIT models. Here, the turbulent transition region has higher uncertainty, possibly due to the changing cell location where transition is manually set.

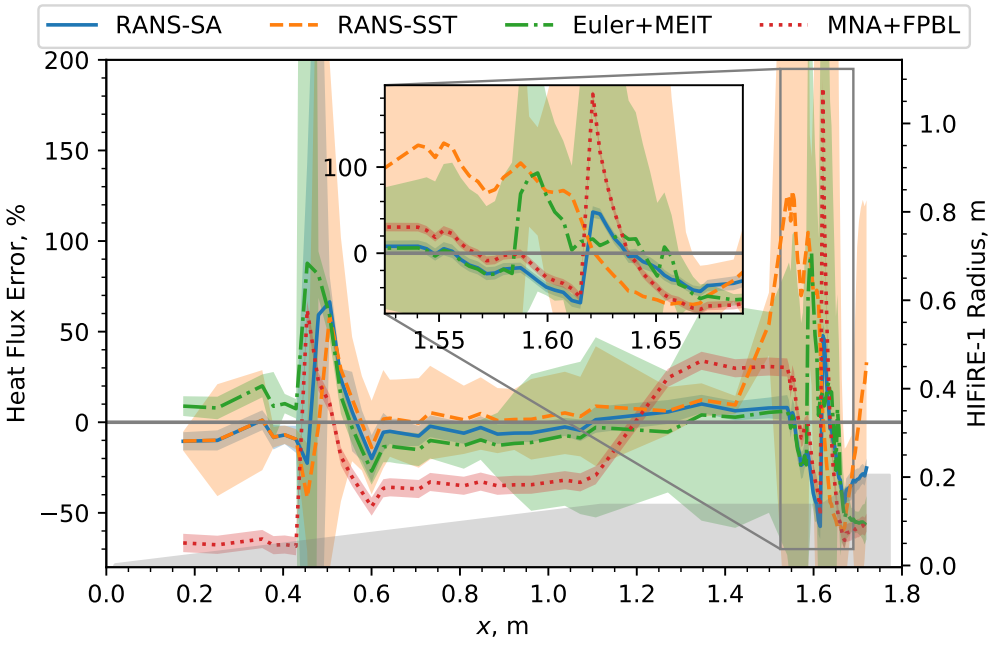

Fig. 8 HIFiRE-1 heat flux prediction error with uncertainty.

Similar to before, the heat flux prediction errors are averaged to provide a better comparison between accuracy of the different models with the results shown in Fig. 9. Figure 9a shows the validation error with the uncertainty only considering the experimental source to better highlight the errors. However, Fig. 9b includes both experimental and numerical uncertainty sources to provide a more complete representation of the relative sizes of the error and uncertainty. Similar to pressure, the RANS-SA model has the smallest error while the RANS-SST and MNA+FPBL models have the largest with a difference of about $2\times$. The lower accuracy of the MNA+FPBL model is expected, but the RANS-SST model was expected to have high accuracy overall. With the more comprehensive validation uncertainty in Fig. 9b, this uncertainty overwhelms the prediction error for the RANS-SST and Euler+MEIT models, suggesting that these models are not mesh-converged.

The prediction errors are again separated into different sections in Fig. 10 with only the experimental uncertainty

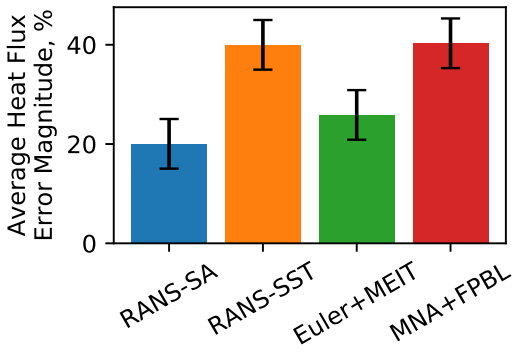

(a) Validation uncertainty only considering experimental source.

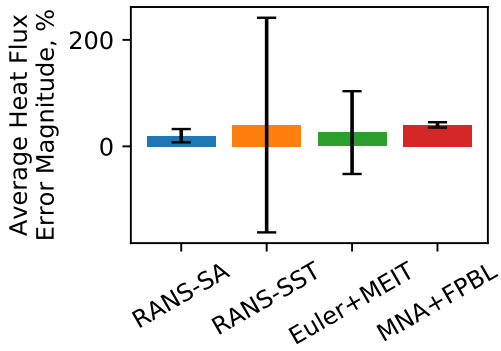

(b) Validation uncertainty considering experimental and numerical sources.

Fig. 9 HIFiRE-1 heat flux prediction error magnitude averaged over data with uncertainty.

considered in Fig. 10a to help resolve errors and the more comprehensive uncertainty treatment in Fig. 10b. On both the laminar and turbulent sections of the cone, the RANS models are most accurate, followed by Euler+MEIT, with MNA+FPBL least accurate as expected. These three higher-fidelity models have higher error in the turbulent cone section than laminar, an expected result from the higher heat flux and modeling challenges inherent with turbulence modeling. In the cylindrical section, the RANS-SST model has the highest prediction error, likely due to the premature separation prediction. As with the cone, the three higher-fidelity models are most accurate in the flare region. When considering both uncertainty terms available in this work, the uncertainty is consistently larger than the error for the RANS-SST and Euler+MEIT models. Further mesh refinement or potentially mesh quality improvements could reduce the numerical uncertainty and help resolve the predictive accuracy.

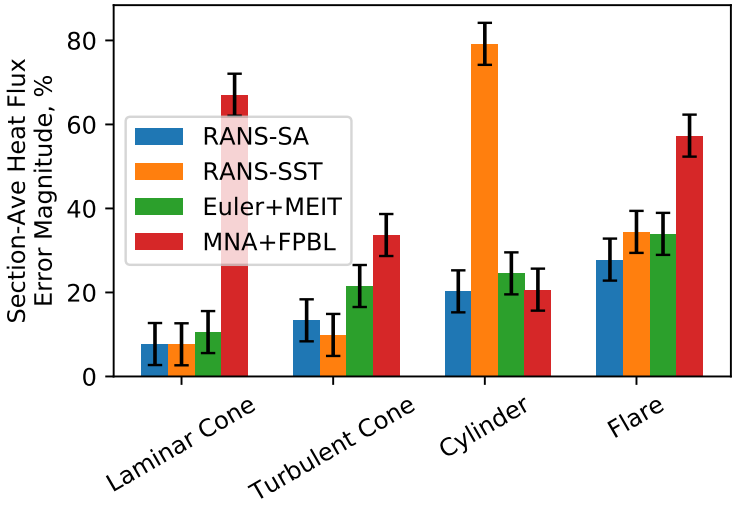

(a) Validation uncertainty only considering experimental source.

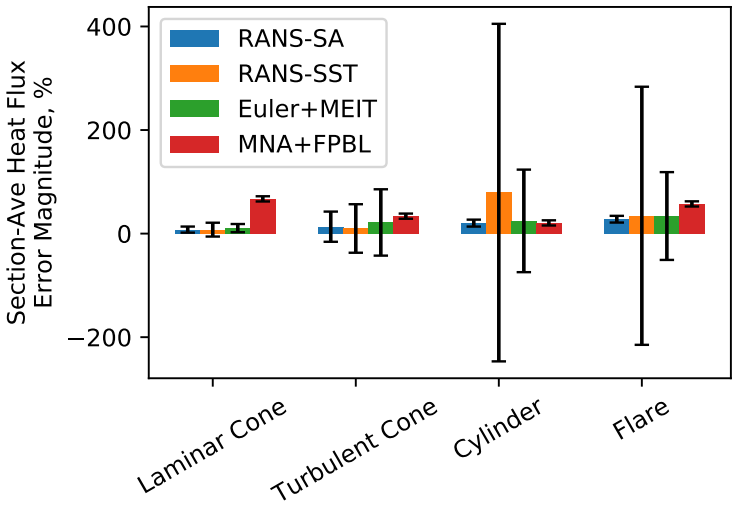

(b) Validation uncertainty considering experimental and numerical sources.

Fig. 10 HIFiRE-1 heat flux prediction error magnitude by section with uncertainty.

V. Conclusion

Herein is the first known validation activities for the Multi-Fidelity Toolkit to provide credibility evidence for its use in high-consequence decision making in hypersonic vehicle analysis at a variety of physics-fidelity and computational-expense levels. It has leveraged best practices in validation applied to all three fidelity levels of MFTK independently.

This work includes a practical description of model validation theory, an overview of the HIFiRE-1 wind tunnel tests, and validation studies of all three fidelity levels of the MFTK at 0° angle of attack. The relative accuracy of the RANS-SA and RANS-SST models is superior for both pressure and heat flux on the laminar and turbulent fore-cone sections of the HIFiRE-1 geometry. The RANS-SA accuracy remains high for the cylindrical and flare sections as well, while the RANS-SST accuracy suffers due to an over-prediction of the separation region. The RANS-SA model had consistently high accuracy and low numerical uncertainty. The Euler+MEIT pressure predictions are second best in general with very reasonable accuracy throughout the domain. For heat flux, the accuracy was second best overall but followed the RANS models for conical performance. The MNA+FPBL model was generally least accurate for both pressure and heat flux; however, it was as accurate as any model on the cylinder as this geometry resembles a flat plate.

With these considerations and recognizing that these accuracies do not directly extrapolate to other parameter spaces of interest, including high-enthalpy or higher-Mach flows, the RANS-SA model is recommended for situations where the highest accuracy is desired with the capability to run more expensive models. The RANS-SST model has accurate predictions for conical flows but is not recommended for separated flows, and has the highest numerical uncertainty in this study. This finding is surprising as the SST model was formulated to perform well in separated flows [16]. The high numerical uncertainty of this model in the separation region deserves further attention. The Euler+MEIT model combination has reasonable accuracy and computational expense but higher than expected numerical uncertainty, an area that deserves further investigation. This mid-fidelity model may be a good fit where the RANS models are too expensive. The iterative stability of the Euler simulations was a challenge with these moderately refined meshes, requiring special attention to the run schedule for complete convergence. The MNA+FPBL models have reasonable accuracy, excellent speed, and negligible numeric uncertainty and may be used where a very high number of simulations is required.

The focus of this work has been on evaluating predictive accuracy through validation with little consideration to performance, a motivator for using MFTK. Nevertheless, the differences in solution speed were notable. While the MNA+FPBL model is solved on a 3D surface mesh for solver convenience, it could theoretically be solved in 2D for this case. Even with this, the speedup is approximately $2{,}000\times$ compared to the RANS-SST model. A more thorough evaluation of the trade-offs between accuracy and speed are recommended for a future work, especially as the faster models enable Monte Carlo uncertainty quantification and design/parameter exploration studies much more readily than the high-fidelity models.

VI. Future Work

This validation study has included a detailed analysis of a single run of the HIFiRE-1 wind tunnel test data set at 0° angle of attack. It will be extended to include cases with nonzero angles of attack and potentially to those at different Reynolds numbers so the predictive accuracy can be quantified under other conditions of interest. Furthermore, other data sets with higher enthalpy flow will be explored to exercise reacting gas models not currently tested with this case. The large magnitude of the numerical uncertainty for the RANS-SST and Euler+MEIT models in the area of separated flow dominates the validation error and should be reduced for more conclusive results. This could be done relatively easily by further mesh refinement. Furthermore, a parameter UQ study could provide added fidelity to the validation uncertainty to help discern validation error from uncertainty.

Acknowledgments

The authors wish to thank Greg Weirs, Derek Dinzl, and Jaideep Ray for their insights into the HIFiRE-1 experiments as well as previous simulations performed at Sandia National Laboratories. The authors also wish to thank Jared Kirsch for his thorough review of the manuscript.

Sandia National Laboratories is a multimission laboratory managed and operated by National Technology & Engineering Solutions of Sandia, LLC, a wholly owned subsidiary of Honeywell International Inc., for the U.S. Department of Energy's National Nuclear Security Administration under contract DE-NA0003525. This paper describes objective technical results and analysis. Any subjective views or opinions that might be expressed in the paper do not

necessarily represent the views of the U.S. Department of Energy or the United States Government. SAND2021-XXXX.

References

[1] Kim, Y., Lee, S., Yee, K., and Rhee, D. H., "High-to-Low Initial Sample Ratio of Hierarchical Kriging for Film Hole Array Optimization," *Journal of Propulsion and Power*, Vol. 34, No. 1, 2018, pp. 108–115. doi: 10.2514/1.B36556.

[2] Krueger, A. M., Lance, B. W., Freno, B. A., and Wagnild, R. M., "Verification Studies of the Multi-Fidelity Toolkit," *AIAA SciTech Forum*, AIAA, 2021.

[3] ASME, "V&V 10-2019: Standard for Verification and Validation in Computational Solid Mechanics," Tech. rep., American Society of Mechanical Engineers, 2020.

[4] Roache, P. J., *Fundamentals of Verification and Validation*, Hermosa publishers, 2009.

[5] Oberkampf, W. L., and Roy, C. J., *Verification and Validation in Scientific Computing*, Cambridge University Press, 2010. doi: 10.1017/cbo9780511760396.

[6] Salari, K., and Knupp, P., "Code Verification by the Method of Manufactured Solutions," Sandia Report SAND2000-1444, Sandia National Laboratories, June 2000. doi: 10.2172/759450.

[7] AIAA, "Guide for the Verification and Validation of Computational Fluid Dynamics Simulations (AIAA G-077-1998 (2002))," , 1998. doi: https://doi.org/10.2514/4.472855.

[8] ASME, "V&V 20-2009: Standard for Verification and Validation in Computational Fluid Dynamics and Heat Transfer," Tech. rep., American Society of Mechanical Engineers, 2009.

[9] Trucano, T. G., Pilch, M., and Oberkampf, W. L., "General Concepts for Experimental Validation of ASCI Code Applications," Tech. Rep. SAND2002-0341, Sandia National Laboratories, Albuquerque, NM (US), 2002.

[10] MacLean, M., Wadhams, T., Holden, M., and Johnson, H., "Ground Test Studies of the HIFiRE-1 Transition Experiment Part 2: Computational Analysis," *Journal of Spacecraft and Rockets*, Vol. 45, No. 6, 2008, pp. 1149–1164.

[11] Wadhams, T., Mundy, E., MacLean, M., and Holden, M., "Ground Test Studies of the HIFiRE-1 Transition Experiment Part 1: Experimental Results," *Journal of Spacecraft and Rockets*, Vol. 45, No. 6, 2008, pp. 1134–1148.

[12] Kimmel, R. L., Adamczak, D., Paull, A., Paull, R., Shannon, J., Pietsch, R., Frost, M., and Alesi, H., "HIFiRE-1 Preliminary Aerothermodynamic Measurements," *AIAA paper*, Vol. 3413, 2011, p. 2011.

[13] Kieweg, S., Carnes, B., Freno, B., Phipps, E., Ridzal, D., Rider, W. J., Smith, T. M., Weirs, V. G., Dinzl, D., Howard, M., Wagnild, R., Fisher, T., Mussoni, E., Arienti, M., and Ray, J., "ASC ATDM FY18 Level 2 Milestone Report: Validation of Hypersonic Turbulence Physics in SPARC (Official Use Only-Export Controlled Information)," Tech. Rep. SAND2018-10261, Sandia National Laboratories, 2018.

[14] Wagnild, R. M., Dinzl, D. J., Bopp, M. S., Dement, D. C., Robbins, B. A., Bruner, C. W. S., Grant, M. J., Murray, J., and Harper, J. M., "Development of a Multi-fidelity Toolkit for Rapid Aerothermal Model Development," Sandia Report SAND2019-13632, Sandia National Laboratories, Oct 2019.

[15] White, F. M., and Corfield, I., *Viscous Fluid Flow*, Vol. 3, McGraw-Hill New York, 2006.

[16] Menter, F. R., Kuntz, M., and Langtry, R., "Ten Years of Industrial Experience with the SST Turbulence Model," *Turbulence, Heat and Mass Transfer*, Vol. 4, No. 1, 2003, pp. 625–632.